Molecular Biology of the Cell
Vol. 10, 1477–1494, May 1999

Association of Myosin I Alpha with Endosomes and Lysosomes in Mammalian Cells

Graça Raposo,* Marie-Neige Cordonnier,* Danièle Tenza, Bernadette Menichi, Antoine Dürrbach, Daniel Louvard, and Evelyne Coudrier†

Morphogenèse et Signalisation Cellulaires, Centre National de la Recherche Scientifique, Unité Mixte de Recherche 144, Institut Curie, 75248 Paris Cedex 05, France

Submitted January 25, 1999; Accepted February 25, 1999
Monitoring Editor: Ari Helenius

Myosin Is, which constitute a ubiquitous monomeric subclass of myosins with actin-based motor properties, are associated with plasma membrane and intracellular vesicles. Myosin Is have been proposed as key players for membrane trafficking in endocytosis or exocytosis. In the present paper we provide biochemical and immunoelectron microscopic evidence indicating that a pool of myosin I alpha (MMIα) is associated with endosomes and lysosomes. We show that the overproduction of MMIα or the production of nonfunctional truncated MMIα affects the distribution of the endocytic compartments. We also show that truncated brush border myosin I proteins, myosin Is that share 78% homology with MMIα, promote the dissociation of MMIα from vesicular membranes derived from endocytic compartments. The analysis at the ultrastructural level of cells producing these brush border myosin I truncated proteins shows that the delivery of the fluid phase markers from endosomes to lysosomes is impaired. MMIα might therefore be involved in membrane trafficking occurring between endosomes and lysosomes.

INTRODUCTION

Most of the membrane-trafficking events in metazoans are driven by microtubule-based molecular motors. However the increase in the number of new unconventional myosins and the recent demonstration that intracellular compartments of mammalian cells move in vivo and in vitro on actin filaments stimulated the investigation of the actin-based membrane trafficking in metazoan organisms (Langford *et al.*, 1994; Evans and Bridgman, 1995; Morris and Hollenbeck, 1995; Bearer *et al.*, 1996; Rogers and Gelfand, 1998). The myosin superfamily encompasses to date at least 14 different classes (Cope *et al.*, 1996; Mermall *et al.*, 1998). Direct evidence for the involvement of specific myosins in membrane trafficking is sparse but indicates that at least four classes of myosins, myosin I, II, V, and VI, are involved in membrane trafficking. Experiments using in vitro assays suggest that myosin II is implicated in post-Golgi transport process from the trans-Golgi network to the cell surface or in the production of constitutive transport vesicles (Musch *et al.*, 1997; Simon *et al.*, 1998). Indirect biochemical, cytological, and genetic evidence suggests that myosin V is involved in organelle movement. (Baker and Titus, 1998; Evans *et al.*, 1998). Myosin VI (95F) has been implicated in cargo transport function in early *Drosophila* embryo (Mermall and Miller, 1995).

The majority of our understanding of the functional properties of myosin Is derived from studies on amoebae and yeast. Unlike the double-headed structure of myosin II or myosin V, myosin Is are single-headed, low-molecular-weight members of the myosin superfamily. Although, all myosin Is exhibit in their tail a positively charged region that has been shown to bind directly to anionic lipids, myosin Is can be divided into distinct subclasses based on sequence homologies in their head and tail domains (Coluccio and Conaty, 1993; Ruppert *et al.*, 1993; Bement *et al.*, 1994). The localization of the members of one subclass of myosin I and the analysis of mutant phenotypes in amoebas, *Saccharomyces cerevisiae*, and *Aspergillus nidulans*, have implicated these motors in cell locomotion, phagocytosis, pinocytosis, and endocytosis (McGoldrick *et al.*, 1995; Novak *et al.*, 1995; Novak and Titus, 1997; Jung *et*

* These authors contributed equally to this work.
† Corresponding author. E-mail address: coudrier@curie.fr.

al., 1996; Geli and Riezman, 1996). The members of this subclass have a tail domain that contains, in addition to the positively charged region, a glycine-, proline-, and alanine-rich region harboring a second actin binding site, and an *src*-homology 3 domain (Goodson and Spudich, 1995; Ostap and Pollard, 1996). It has been postulated that this subclass of myosin I might cross-link the actin filaments via their two actin binding sites (the ATP-dependent site located in the head and the ATP-independent site in the tail) and control thereby the dynamic state of the actin-rich cortex required for these different functions (Goodson *et al.*, 1996; Ostap and Pollard, 1996).

In contrast, the members of the subclass that encompasses myosin I alpha (MMIα) and brush border myosin I (BBMI) exhibit a tail with only the putative membrane binding domain (Ruppert *et al.*, 1993; Sheer *et al.*, 1993). This subclass of proteins has been found to date only in metazoans. The subcellular distribution of this subclass of myosin I suggested that it might be involved in membrane trafficking. Indeed, these proteins have been localized at the cell periphery (in the microvilli of intestinal cells in the case of BBMI, in the plasma membrane of normal rabbit kidney cells in the case of Myr 1, and in the growth cone of nerve cells in the case of MMIα), and in association with intracellular membrane (membrane vesicles in the terminal web of intestinal cells in the case of BBMI and tubular structures of the cell body of neurons in the case of MMIα) (Ruppert *et al.*, 1995; Lewis and Bridgman, 1996; Drenckhahn and Dermietzel, 1988).

We previously reported that membrane trafficking during endocytosis required actin filaments for the uptake of ligands and for their delivery to the lysosomes (Durrbach *et al.*, 1996b). We also suggested that the production of BBMI lacking the entire motor domain or the amino-terminal sequence containing the ATP binding site, in a hepatoma cell line, had a dominant negative effect on the endocytic pathway by competing with an endogenous myosin I (Durrbach *et al.*, 1996a). We have pursued these observations and demonstrated in this report that MMIα is the myosin I associated with endocytic compartments. Biochemical and immunocytochemical analyses show that MMIα is associated with endosomes and lysosomes. The overproduction of MMIα or the production of nonfunctional truncated MMIα affects, similarly to the truncated BBMI proteins, the distribution of the endocytic compartments. In vitro assays indicate that the truncated BBMI proteins can compete with the binding of MMIα to the vesicular membranes derived from endocytic compartments. Analysis at the ultrastructural level of the cells producing the truncated proteins showed that they were unable to deliver properly the fluid phase markers from endosomes to lysosomes. Altogether our observations further support our earlier hypothesis for a role of a myosin I in the endocytic pathway.

MATERIALS AND METHODS

Antibodies

We used monoclonal antibodies directed against the motor domain and the tail domain of the chicken BBMI, CX-1, and CX-7 (Carboni *et al.*, 1988) and polyclonal antibodies directed against Myr 1 and referred to Tu 30 and Tu 22 (Ruppert *et al.*, 1993, 1995). Tu 30 was raised against the Myr 1 amino terminus, and Tu 22 was raised against a synthetic peptide of the Myr 1 tail (Ruppert *et al.*, 1993). We also used polyclonal antibodies directed against rab 5 (Chavrier *et al.*, 1990), polyclonal antibodies directed against the cytoplasmic tail of the lysosomal membrane glycoprotein (lgp 120) (Bakker *et al.*, 1997), monoclonal antibody directed against the Golgi complex (Jasmin *et al.*, 1989), monoclonal antibody directed against rab 7 (Meresse *et al.*, 1995), polyclonal antibodies directed against cathepsin D (Bailly *et al.*, 1991), and monoclonal antibody H68.4 directed against the cytoplasmic tail of transferrin receptor according to White *et al.* (1992). Polyclonal antibodies directed against β-actin were a generous gift from C. Chaponnier (Geneva University, Geneva, Switzerland). Monoclonal antibody directed against LAMP-1 was obtained from PharMingen (Los Angeles, CA), and antibody directed against HRP was from Sigma (St. Louis, MO).

Cell Culture

The mouse hepatoma cell line BWTG3 (Szpirer and Szpirer, 1975) or cellular clones producing BBMI, BBMIΔ446, BBMI-Tail, or mock cells (cells transfected with the vector without insert) described by Durrbach *et al.* (1996a) were grown at 37°C under 10% CO_2 in Coon's F-12 modified medium (Seromed, Berlin, Germany) supplemented with 10% FCS (Seromed) and penicillin (10 U/ml) and streptomycin (10 μg/ml) (Seromed) in the case of the BWTG3 cells or supplemented with 0.7 mg/ml Geneticin, (Life Technologies, Paisley, Scotland) in the case of mock cells or the cellular clones producing BBMI or the truncated BBMI proteins.

Immunoprecipitation, Immunoblotting, and Mass Spectrometry Analysis

Immunoprecipitation. Cells were grown 2 d on a 10-cm Petri dish and lysed in 1 ml of 10 mM Tris, pH 7.4, containing 150 mM NaCl, 1% Triton X-100, 0.5% deoxycholate, and 0.1% SDS (immunoprecipitation buffer) on ice. After centrifugation for 10 min at 10,000 $\times$ *g*, the cell lysate was preabsorbed on 50 μl of protein A-Sepharose beads (Pharmacia Biotech, Uppsala Sweden). The immunocomplex formed overnight at 4°C by incubating the cell lysate with 20 μl of sera or ascites fluid was absorbed on 20 μl of protein A-Sepharose and washed six times with the immunoprecipitation buffer and once with 10 mM Tris, pH 7.4, and 150 mM NaCl. Each sample was analyzed by SDS-PAGE and processed for immunoblotting or stained with Coomassie Blue dye.

Immunoblotting. Proteins separated by SDS-PAGE were transferred on nitrocellulose membranes in the presence of 20 mM Tris, 150 mM glycine, and 0.0375% SDS. Detection of antibodies was performed using the chemiluminescence blotting substrate from Boehringer Mannheim (Mannheim, Germany). The relative amount of proteins immunodetected was quantified by scanning densitometry using the Bio-Profil system (Vilber Lourmat, Marne la Vallée, France).

Mass Spectrometry Analysis. The gel bands containing the 130-kDa protein stained by Coomassie Blue dye were washed, dried, and submitted to trypsin proteolysis according to the method of Shevchenko *et al.* (1996). The supernatant (0.5 ml) was mixed on the

target of the mass spectrometer with 0.5 ml of a saturated solution of 2,5-dihydroxybenzoic acid in 0.1% aqueous trifluoroacetic acid. Peptide molecular weights were determined by matrix-assisted laser desorption and ionization–time of flight analysis. Spectra were obtained in positive reflection mode on a Voyager Elite matrix-assisted laser desorption and ionization–time of flight mass spectrometer (Perceptive Biosystems, Framingham, MA) equipped with a delayed extraction device. The peptides maps identified with this method have been compared with the OWL, European Molecular Biology Laboratory, and Swiss data bases.

Immunofluorescence Microscopy

For immunofluorescence analysis cells were grown 2 d on coverslips and incubated overnight in cell culture medium containing 10 mM sodium butyrate in the case of stable cell lines producing BBMI, BBMIΔ446, or BBMI-Tail.

Internalization of Transferrin. Cells were washed three times with RPMI 1640 medium followed by a 30-min incubation period with RPMI 1640 medium at 37°C. The cells were then incubated 20 min at 37°C with biotinylated transferrin at 20 μg/ml (Sigma) in RPMI 1640 medium. Then cells were washed three times with cold RPMI 1640 medium containing 0.1 mg/ml BSA and processed for immunofluorescence analysis. Biotinylated transferrin was detected with streptavidin-conjugated with Texas Red from Molecular Probes (Eugene, OR).

Indirect Immunofluorescence Analysis. Cells were fixed with 3% paraformaldehyde and 0.025% glutaraldehyde, permeabilized with PBS containing 0.1% saponin, and analyzed by indirect immunofluorescence. Cells were first incubated 30 min with primary antibodies, followed by 30 min with TRITC- or FITC-conjugated secondary antibodies (Cappel). Phalloidin (0.5 μg/ml) conjugated to either TRITC (Sigma) or FITC (Sigma) was used to label F actin. Cells were viewed with a confocal laser scanning microscope (Leica, Vienna, Austria).

Electron Microscopy

Internalization of HRP. Cells producing BBMI, BBMIΔ446, or BBMI-Tail or mock cells were incubated overnight with sodium butyrate (10 mM) and washed with RPMI 1640 medium without FCS. The cells were allowed to internalize type II HRP (Sigma) at a final concentration of 10 mg/ml for 40 min at 37°C. After cooling on ice, cells were washed four times with RPMI 1640 medium containing 5% FCS. Cells were fixed with a mixture of 2% paraformaldehyde and 1% glutaraldehyde in 0.2 M phosphate buffer, pH 7.4, for 1 h at room temperature and washed with 50 mM Tris buffer, pH 7.6. The diaminobenzidine (DAB) reaction proceeded for 20 min with 0.003% DAB and 1 μl/ml H_2O_2 (30 vol). Cells were post-fixed with OsO_4, dehydrated in ethanol, and embedded in Epon. Ultrathin sections were counterstained with uranyl acetate and viewed with an electron microscope (CM120 TEM; Phillips, Eindoven, The Netherlands).

Ultracryomicrotomy and Immunogold Labeling. Cells were allowed to internalize HRP as described above and processed for ultracryomicrotomy after the fixation step. They were removed from the dish by gentle scraping, washed with 0.2 M phosphate buffer, pH 7.4, containing 0.1 M glycine, and embedded in gelatin. Small gelatin blocks were infused in 2.3 M sucrose and frozen in liquid nitrogen. Ultrathin cryosections were prepared with a diamond knife (Drukker, Biel, The Netherlands) and an ultracryomicrotome (Ultracut UCT; Leica). Ultrathin freeze–thaw sections were immunogold labeled with the different antibodies and with protein A-gold conjugates (purchased from Dr. J. W. Slot, Department of Cell Biology, University of Utrecht, Utrecht, The Netherlands) (Slot *et al.*, 1991; Raposo *et al.*, 1997). To determine the distribution of HRP in lysosomes (cathepsin D-positive compartments), the number of HRP- and cathepsin D-positive compartments was counted by electron microscopy (EM) imaging. For each clone 30 cellular profiles were analyzed, and compartments showing >10 gold particles for cathepsin D were considered as lysosomes.

Whole-Mount EM. Immunogold labeling on entire BWTG3 cells was performed as described by Stoorvogel *et al.* (1996). Cells were grown for 2 d on Formvar-coated gold grids, washed with minimum essential medium and 20 mM HEPES, and allowed to internalize for 2 h in type II HRP (Sigma) at a final concentration of 7 mg/ml. Cells were rapidly cooled at 0°C and washed with minimum essential medium and 20 mM HEPES. The endocytic compartments containing internalized HRP were cross-linked by incubation for 30 min at 0°C in 1.5 mg/ml DAB, 70 mM NaCl, 50 mM ascorbic acid, 20 mM HEPES, and 0.02% H_2O_2. After removing the excess of DAB by extensive washing with 80 mM piperazine-*N*,*N*′-bis(2-ethanesulfonic acid) buffer, pH 7, at 0°C, cells were permeabilized with a buffer containing 80 mM piperazine-*N*,*N*′-bis(2-ethanesulfonic acid), pH 7, 0.1 mM EGTA, 0.5 mM $MgCl_2$, 0.5 mg/ml saponin, and 5 mM ascorbic acid. Cells were then fixed with a mixture of 2% paraformaldehyde and 0.2% glutaraldehyde, quenched with 50 mM NH_4Cl in PBS, and immunogold labeled with the different antibodies and protein A-gold. After immunogold labeling, cells were fixed with 2% glutaraldehyde, rinsed with water, dehydrated with increasing concentrations of ethanol, and critical point dried in a critical point dry apparatus (Balzers, Liechtenstein).

Endosomal Fractions. Fractions were fixed with 2% paraformaldehyde in 0.2 M phosphate buffer, pH 7.4, and loaded onto Formvar-carbon–coated EM grids. After washing with PBS and 50 mM glycine, whole-mounted fractions were immunolabeled, contrasted, and embedded as described for ultrathin cryosections and for whole-mounted membrane vesicles (Raposo *et al.*, 1996, 1997).

Cell Homogenate and Membrane Fractionation

Cells were grown 5 d on 175-cm^2 flasks, collected by scraping, and resuspended in 1 ml of homogenization buffer containing 10 mM triethanolamine, pH 7.4, 0.25 M sucrose, 1 mM EDTA, and protease inhibitors (0.2 mM PMSF, 1 mM pepstatin, 1 mM benzamidine, and 1 mM aprotinin). Then they were homogenized by passing them in a cell cracker. Unbroken cells and nuclei were removed from the cell homogenate by centrifugation at 1000 × *g* for 10 min, and the crude membrane fraction contained in the postnuclear supernatant was resuspended in 1.18 M sucrose loaded under a layer of 1 M sucrose and a layer of 0.25 M sucrose according to the method of Gorvel *et al.* (1991). The gradient was centrifuged 1 h at 130,000 × *g*. The fraction enriched in endocytic compartments was collected at the interface of 1 and 0.25 M sucrose. Alternatively, the postnuclear supernatant was loaded in 25% Percoll on a 1 M sucrose cushion according to the method of Green *et al.* (1987) and centrifuged 20 min at 22,500 × *g*.

Recombinant cDNA Constructions

The recombinant plasmid encoding green fluorescent protein (GFP)-Myr 1 was obtained by inserting myr 1 cDNA (PIR data bank accession number 45439) downstream the oligonucleotide (catgggtggatatctaggatccg) in the *Eco*RI–*Sal*I restriction sites of the pEGFPc1 plasmid (Clontech, Palo Alto, CA). In this construct the 5′ end of myr 1 cDNA was located downstream of the 3′ end of the GFP cDNA. The expression of the recombinant plasmid leads to the addition of 18 amino acids (SGLRSRAQASNSPDRYPP) between GFP and Myr 1. The recombinant plasmid encoding GFP-Myr1Δn295 was obtained by deleting the fragment *Bam*HI–*Bam*HI from the recombinant plasmid encoding GFP-Myr 1. The expression of the recombinant plasmid leads to the addition of 12 amino acids (SGLRSRAQASNS) between the GFP protein and Myr 1 truncated

protein (aa 296-1041). The recombinant plasmid encoding GFP-Myr 1-Tail was obtained by deleting the fragment *Eco*RV-*Eco*RV from the recombinant plasmid encoding GFP-Myr 1. The expression of the recombinant plasmid leads to the addition of 15 amino acids (SGLRSRAQASNSPDR) between the GFP protein and Myr 1-Tail (aa 747-1041).

The recombinant plasmid encoding GST-BBMIΔ446 (aa 446-1040) was obtained by subcloning the cDNA encoding BBMIΔ446 into the *Sma*I–*Eco*RI restriction sites of the pGEX2T plasmid (Durrbach *et al.*, 1996a). This protein is deleted of the first 445 amino acids that encompass the domain that harbors the ATP binding site. The recombinant plasmid encoding the GST-Tail (aa 730-1040) was obtained by subcloning the cDNA encoding the tail and the oligonucleotide (5′-GATCCTCCCACGCCTGCA-3′) into the *Bam*HI restriction site of the pGEX2T plasmid (Durrbach *et al.*, 1996a). This protein is deleted of the first 729 amino acids that encompass the entire motor domain.

Transfection

Five million trypsinized BWTG3 cells were electroporated at 250 V and 0.960 mF in 200 μl of Coon's F-12 modified medium containing 1 mM HEPES, pH 7.5, and 10 μg of recombinant plasmid. After dilution in complete culture medium cells were plated on coverslips and analyzed 24 h later.

Purification of the Recombinant GST Fusion Protein

Escherichia coli transformed with pGEX2T-BBMIΔ446 or pGEX2T-Tail were grown in 500 ml of Luria–Bertani medium and 100 μg/ml ampicillin and induced 30 or 15 min, respectively, for BBMIΔ446 and BBMITail with 1 mM isopropyl-1-thio-β-D-galactopyranoside. Cells were lysed by sonication in 10 ml of PBS containing 1% Triton X-100. The lysate was then incubated overnight at 4°C with glutathione-Sepharose 4B (Pharmacia Biotech), and the GST fusion proteins were eluted by 10 mM glutathione in the presence of 0.1 mg/ml calmodulin for GST-BBMIΔ446.

RESULTS

Detection of MMIα in Mouse Hepatoma Cells (BWTG3)

We first attempted to identify a myosin I in the mouse hepatoma cell line using two antibodies, one directed against an epitope of the motor domain of BBMI and the second directed against the amino terminus of MMIα. We show in Figure 1A, lanes 1–3, that a 130-kDa protein is detected with a monoclonal antibody directed against the head domain of BBMI (CX-1) in samples from mouse liver, total homogenate of the mouse hepatoma cell line (BWTG3), and the postnuclear supernatant of these cells. Mouse MMIα, identical to Myr 1 of rat, shares 78% sequence homology with BBMI and has a size compatible with the apparent molecular mass of this protein. Indeed the anti-Myr 1 antibodies (Tu 30) also recognize a 130-kDa protein in the same samples (Figure 1A, lanes 4–6). Both antibodies also immunoprecipitated specifically a 130-kDa protein from BWTG3 cell homogenate (Figure 1B). The 130-kDa protein immunoprecipitated with the anti-BBMI antibody was detected with the anti-Myr 1 antibody by Western blot analysis (Figure 1B, lane 2). The 130-kDa protein was not fully immunoprecipitated with the anti-BBMI antibody in our experiments. The remaining 130-kDa protein can be recognized on the blots by anti-BBMI antibody (Coudrier, unpublished data) and anti-Myr 1 antibodies (Figure 1B, lane 3). This remaining protein was immunoprecipitated with the anti-Myr 1 antibodies and detected by Western blot with the anti-Myr 1 and anti-BBMI antibodies (Figure 1B, lanes 4 and 6). After the second immunoprecipitation the 130-kDa protein was hardly detectable in the remaining supernatant (Figure 1B, lane 5). These data strongly suggest that both antibodies recognize the same protein, which has an apparent molecular mass compatible with the size of MMIα (Ruppert *et al.*, 1993; Sheer *et al.*, 1993).

To identify the protein recognized by these antibodies, we analyzed the composition of the 130-kDa protein immunoprecipitated with anti-Myr 1 antibodies after trypsin digestion and mass spectrometry analysis. We resolved 27 peptides. The size of 13 of them matched the size of 16 peptides that can be theoretically generated by trypsin proteolysis of Myr 1c and MMIα (Figure 1C). These peptides covered 15% of the entire sequence of MMIα (Figure 1D). Thus, anti-Myr 1 antibodies (Tu 30) immunoprecipitate the MMIα in the mouse hepatoma cell line BWTG3. A similar analysis with the 130-kDa protein immunoprecipitated with anti-BBMI antibody showed that this antibody also recognized MMIα.

MMIα Codistributes Partially with Endocytic Compartments

We studied the distribution of MMIα in the BWTG3 cells by indirect immunofluorescence using the above-characterized anti-Myr 1 antibodies. As previously observed by others (Coluccio and Conaty, 1993; Ruppert *et al.*, 1995; Lewis and Bridgman, 1996), we have detected MMIα near the plasma membrane in regions enriched for actin filaments (Figure 2, A and B). In addition we observed a punctate staining throughout the cytoplasm with an intense cap at one pole of the nucleus. Actin filaments were also enriched in the perinuclear region of this cell line (Figure 2A). A similar distribution was observed using another anti-Myr 1 antibody raised against a peptide from the tail of Myr 1 (Tu 22) (Figure 2D). The detection of MMIα in the perinuclear region is in agreement with the previous observations from Coluccio and Conaty (1993) on rat liver. It is well established that in this region, the Golgi apparatus and late and recycling endocytic compartments are usually codistributed. In Figure 2, C and D, we show that MMIα codistributes partially with fluorescent transferrin internalized within 20 min. To distinguish endosomal membranes from Golgi membranes by immunofluorescence analysis, we used a procedure described by Stoorvogel *et al.* (1996). This method, developed to analyze the struc-

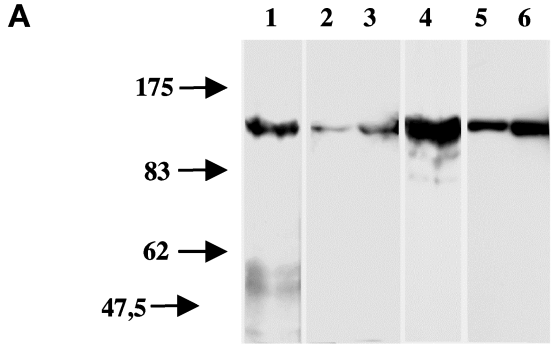

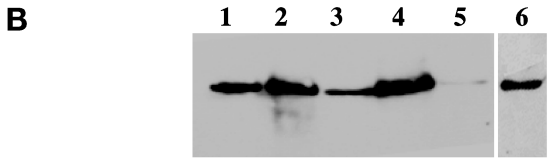

C

Peptide maps	Peptides from MMIα		
Size(Da)		Start	End
869.99	IFHLWR	860	865
1033.74	LFSWLVNR	361	368
	TTLSQTKQK	1023	1031
1044.74	THFLLMKR	723	730
	EYRKFFR	799	805
1058.49	SLFPEGNPAK	553	562
1075.79	YLGLLENVR	619	627
1172.79	YNYLSLDSAK	232	241
1191.79	SQVVIAAWYR	731	740
1235.69	SSALVIQSYIR	753	763
1380.87	IIIAEVVNKINR	930	941
1606.84	FLNDTTLPHSCFR	500	512
	SSALVIQSYIRGWK	753	766
1676.99	FIQGNQKNGSVPTCK	1053	1067
1695.04	SLPIYSPEKVEDYR	60	73
2185.69	ENSYNFDQLLEQKQQMRS	646	662

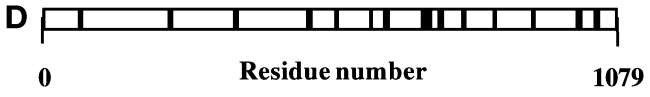

Figure 1. Antibodies directed against BBMI and Myr 1 recognize MMIα in the BWTG3 cells. (A) Twenty micrograms of proteins from mouse liver homogenate (lanes 1 and 4), total BWTG3 cell homogenate (lanes 2 and 5), and postnuclear supernatant (lanes 3 and 6) were separated by 7% SDS-PAGE, and transferred to nitrocellulose membranes. The membranes were probed with a monoclonal antibody directed against BBMI head domain (CX-1; lanes 1–3), or with anti-Myr 1 antibodies (Tu 30; lanes 4–6). (B) Western blot analysis of BWTG3 cell lysate immunoprecipitated with a monoclonal antibody directed against BBMI head domain (CX-1) or the antibodies directed against Myr 1 (Tu 30). Total cell lysate (lane 1), total cell lysate immunoprecipitate with anti-BBMI antibody (lane 2), supernatant of the cell lysate after the immunoprecipitation with anti-BBMI antibody (lane 3), supernatant immunoprecipitate with anti-Myr 1-antibodies (Tu 30; lanes 4 and 6), and supernatant after immunoprecipitations with both antibodies (lane 5) were separated by 7% SDS-PAGE and transferred to nitrocellulose membranes. The membranes were probed with anti-Myr 1 antibodies (Tu 30; lanes 1–5) and with the anti-BBMI antibody (CX-1; lane 6). (C) The peptide map derived from the trypsin proteolysis of the 130-kDa protein immunoprecipitated with anti-Myr 1 was compared with the OWL data base using a Baysien algorithm (Profound). Thirteen peptides matched 16 peptides of MMIα. (D) Distribution of matched peptides along the sequence of MMIα. Note that the majority of the peptides were located on the tail sequence that diverges more from one subclass of myosin I to another.

ture of endosomes at the electron microscopic level and to immunolocalize proteins associated with their cytoplasmic side, allows preservation of endocytic compartments after cross-linking by DAB cytochemistry. In contrast, cytosolic components and membrane compartments that have not been filled with HRP, namely the Golgi complex, are extracted during the permeabilization procedure performed before fixation. In these conditions, we were still able to observe a punctate staining with anti-MMIα antibodies that codistributed with the transferrin receptor in the perinuclear region, whereas antigen associated with Golgi membrane was hardly detected (Figure 2, E and F vs. G and H). With this method we could also detect actin filaments at the cell periphery and in the perinuclear region (Figure 2I). MMIα codistributes with actin filaments in both regions (Figure 2, I and J). Although these observations do not allow us to exclude that a fraction of MMIα colocalizes with Golgi membranes, they show that a fraction of MMIα is localized at the cell periphery, and another one colocalizes in the perinuclear region with structures recognized as endocytic compartments.

MMIα Is Associated with the β-Actin–rich Cytoskeleton and with Endocytic Compartments

We then analyzed the distribution of MMIα on hepatoma cells, which had been cultured directly on Formvar-coated EM grids by immunoelectron microscopy using the above described method (Stoorvogel *et al.*, 1996). Using such a whole-mount procedure, DAB-positive tubular and vesicular structures associated with a network of filamentous structures were observed (Figure 3A, inset). Filamentous structures located at the leading edge were immunogold labeled with anti-Myr 1 antibodies (Figure 3A). A double labeling allowing the concomitant visualization of MMIα and actin microfilaments using an anti-β-actin polyclonal antibody revealed that the filamentous network with which MMIα associates is highly enriched for actin (Figure 3B). We then focused our attention on the tubular and vesicular structures cross-linked by DAB cytochemistry, which are located at the cell periphery. In agreement with the previous observations

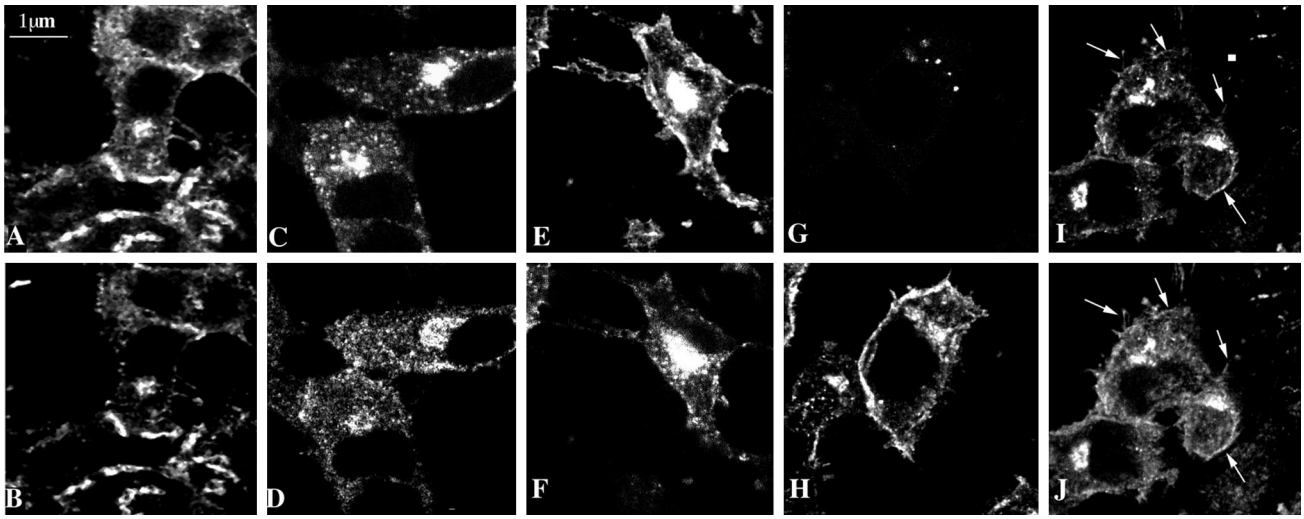

Figure 2. Subcellular distribution of MMIα in BWTG3 cells by confocal immunofluorescence analysis. Paraformaldehyde-fixed and saponin-permeabilized cells were double labeled with phalloidin (A) and anti-Myr 1 antibodies (Tu 30; B). Cells were incubated with biotinylated transferrin 20 min before fixation, permeabilized with saponin, and double labeled with Texas Red-streptavidin (C) and anti-Myr 1 antibodies (Tu 22; D). Note that two antibodies directed against two different domains of Myr 1 decorated similarly punctate structures in the perinuclear region. After preservation of the endocytic compartments according to the procedure of Stoorvogel *et al*. (1996) (see MATERIALS AND METHODS), cells were paraformaldehyde fixed, detergent permeabilized, and double labeled with anti-Myr 1 antibodies (Tu 30; F, H, and J) and antibody directed against the transferrin receptor (H68.4; E), Golgi complex (G), and β actin (I). Horizontal optical sections throughout the focal plane of the nucleus were obtained by confocal laser scanning microscopy.

of Stoorvogel *et al*. (1996), the tubulo-vesicular structures and small vesicles at the cell periphery were decorated with antibodies directed against the cytoplasmic tail of the transferrin receptor (Figure 4A). These endosomal compartments were also intensely labeled with the anti-Myr 1 antibodies (Figure 4B). Double immunogold labeling with anti-Myr 1 antibodies and the anti-transferrin receptor antibody confirmed the association of MMIα with enriched DAB-positive tubulo-vesicular endosomes (Figure 4C). The peripheral tubulo-vesicular structures immunogold labeled with the anti-Myr 1 antibodies showed only a faint labeling with antibodies directed against the cytoplasmic domain of the lysosomal marker lgp 120, whereas intense labeling with the anti-lgp antibodies was observed in large vesicular structures likely identifiable as lysosomal compartments. Interestingly, labeling with the anti-Myr 1 antibodies was also observed in such lysosomal compartments, although, when compared with the endosomal network the labeling was less intense (Figure 4C, inset). This analysis at the ultrastructural level shows the codistribution of MMIα with actin filaments at the cell periphery and with endocytic structures identified as endosomes and lysosomes.

MMIα Is Associated with Membrane Fractions Enriched in Endocytic Compartments

To obtain further evidence of the association of MMIα with endosomes and lysosomes, we next analyzed the distribution of MMIα after cell fractionation. MMIα was hardly detectable in the soluble cytosolic fraction obtained after centrifugation of the postnuclear supernatant at 100,000 × *g* (Figure 5A). The large majority of this protein was instead recovered in the pellet, indicating that MMIα was associated with cellular membranes and/or actin cytoskeleton that binds to these membranes. We have been unable to detect MMIα on vesicular membrane fractions isolated according to the method of Futerman *et al.* (1990) and enriched for markers specific for the Golgi complex (our unpublished results). We separated the membrane vesicles contained in the postnuclear supernatant on a three-step sucrose gradient. Under these conditions MMIα was highly enriched with the membrane fraction that was also enriched for the specific markers of the endocytic compartments such as transferrin receptor, the small GTPases rab 5 and rab 7, and LAMP-1 (Figure 5B).

Because we could not exclude that this membrane fraction was contaminated by plasma membrane, we attempted to separate endosomes from plasma membrane vesicles and from lysosomes by Percoll gradient. Plasma membrane vesicles characterized by alkaline phosphodiesterase activity were collected mainly in fractions 10–12, whereas lysosomes characterized by the β-hexosaminidase activity were collected in the fractions 1–4 (Figure 5C). We combined the fractions of the gradient in three pools, and we analyzed them by Western blotting with specific markers for endo-

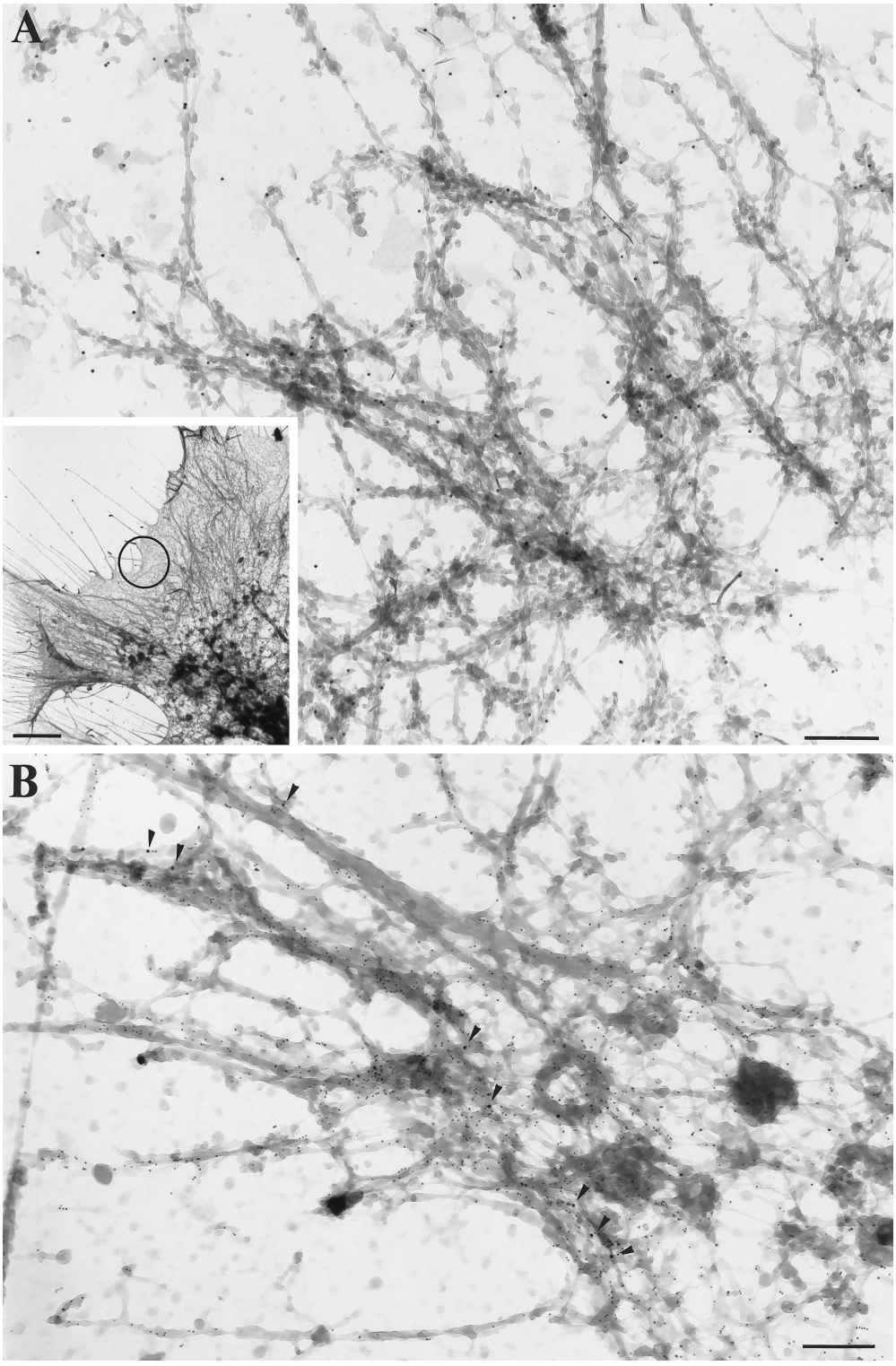

Figure 3. Visualization of MMIα and β-actin by whole-mount EM. (A) Inset, Low magnification (bar, 2 μm) of a filamentous network in the leading edge of BWTG3 cells. DAB-positive tubular and vesicular structures were observed throughout this region, but they were highly concentrated in the distal part of the leading edges. (A) Higher magnification of the circled area in inset. The anti-Myr 1 antibodies (Tu 30; PAG 10) labeled filamentous structures (A). Such a filamentous network to which MMIα (PAG 10; arrowheads) localizes was also immunogold labeled with anti-β-actin antibodies (PAG 5; panel B). (A-B) Bars, 200 nm.

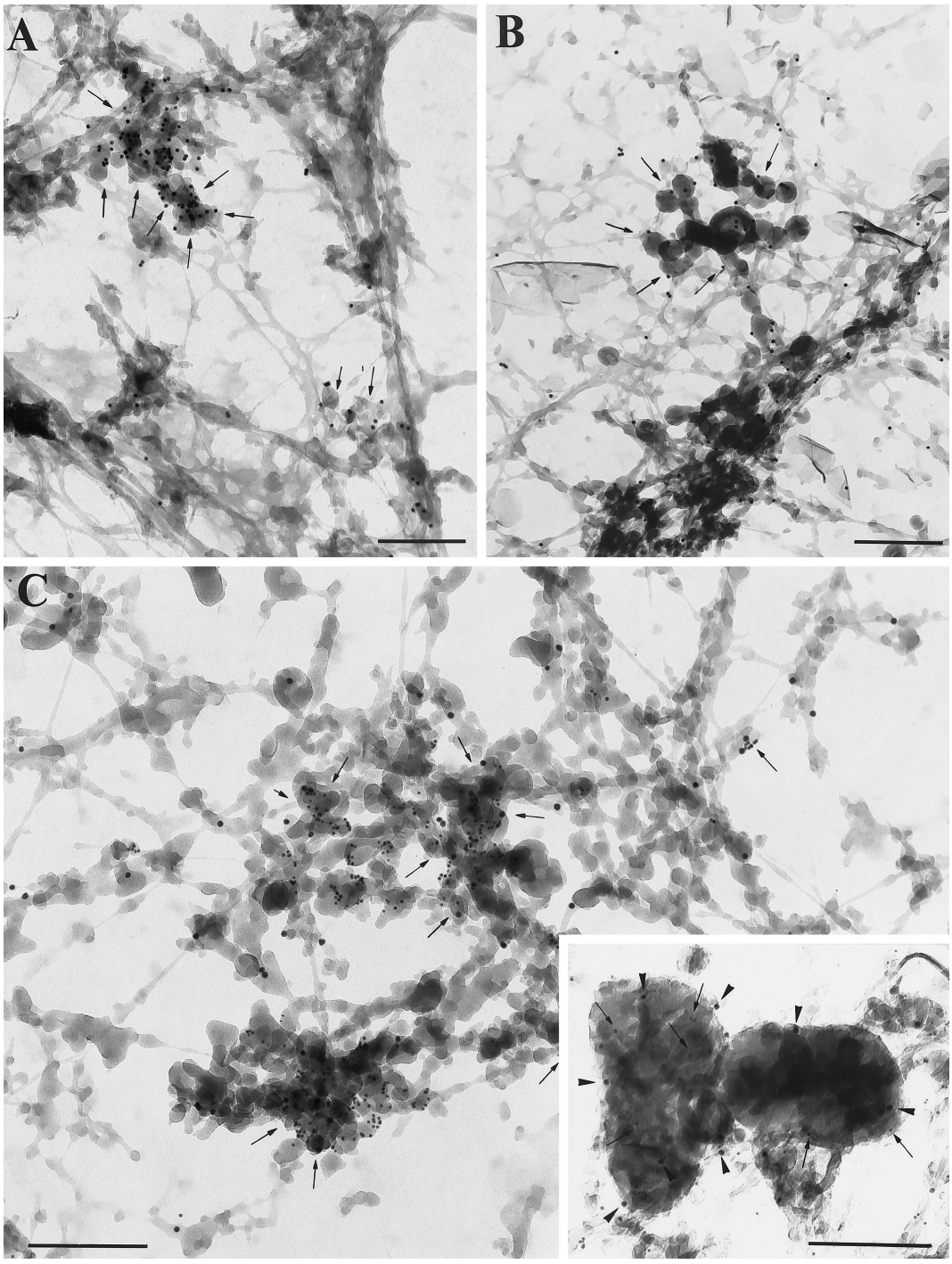

Figure 4. Visualization of MMIα, the transferrin receptor and lgp 120 by whole-mount EM. (A) DAB-positive tubulo-vesicular structures were intensely labeled with the anti-transferrin receptor antibody (H68.4) directed against its cytoplasmic tail (PAG 10; arrows). (B) Similar DAB-positive tubulo-vesicular structures (endosomes) were labeled with the anti-Myr 1 antibodies (PAG 10, Tu 30; B, arrows). (C) Double immunogold labeling with the anti-Myr 1 antibodies (PAG 10) and the anti-transferrin receptor antibody (PAG 5) showed the codistribution of MMIα and transferrin receptor in the same tubulo-vesicular structures (arrows). (C) Inset, Lgp 120 (PAG 5) was detected in DAB-positive lysosomal compartments (arrows), which were also labeled with the anti-Myr 1 antibodies (PAG 10) (arrowheads). Bars, 200 nm.

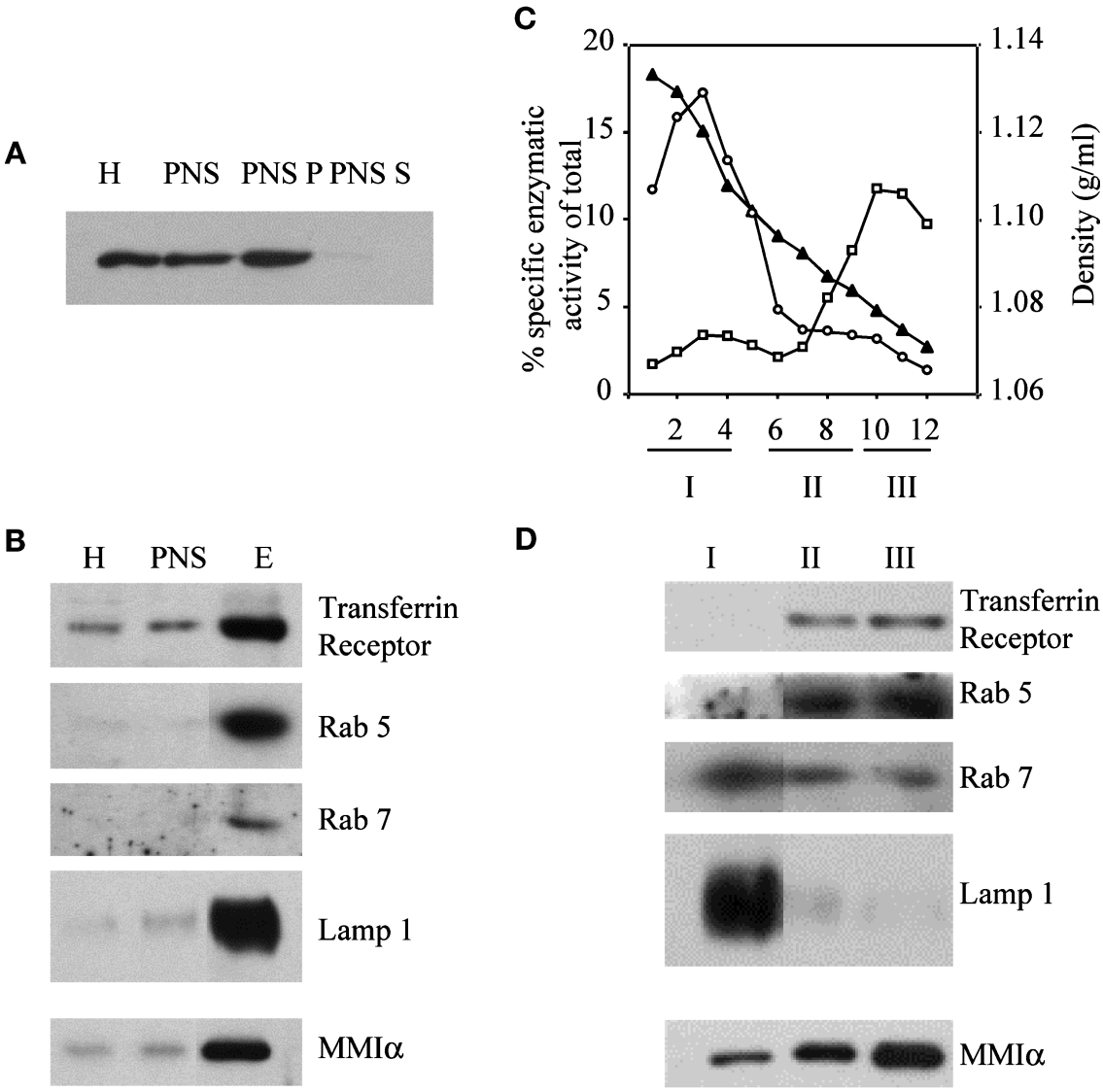

Figure 5. Detection of MMIα in subcellular fractions of BWTG3 cells isolated by a sucrose step gradient or Percoll gradient. (A and B) Five micrograms of proteins from BWTG3 homogenate (H), postnuclear supernatant (PNS), and fractions collected on a three-step sucrose gradient at the interface of sucrose 1 and 0.25 M (E) were separated by 7% SDS-PAGE and transferred on nitrocellulose membranes. (A) Five micrograms of postnuclear supernatant were centrifuged 30 min at 300,000 × *g*. Proteins from the pellet (PNS P) and from the supernatant (PNS S) were analyzed under the same conditions. The membranes were probed with anti-Myr 1 antibodies (Tu 30; A), anti-transferrin receptor (H68.4), anti-rab 5, anti-rab 7, anti-LAMP-1, and anti-Myr 1 (Tu 30) antibodies (B). (C) Fractions collected after separation by Percoll density gradient of the postnuclear supernatant from BWTG3 cells were assayed for β-hexosaminidase (○, lysosomes), and alkaline phosphodiesterase (□, plasma membrane) activities. The linearity of percoll density after centrifugation was measured by refractometry (▲). Further analyses were always restricted to the linear part of the gradient. The graph shows enzymatic activities that correspond to the average of the activity of four fractions with the same position on four Percoll gradients performed at the same time. (D) The fractions of the four gradients were combined into three pools as indicated below the graph. Five micrograms of proteins of each pool were loaded on 7 and 10% SDS-polyacrylamide gels and analyzed by immunoblotting with the anti-transferrin receptor (H68.4), anti-rab 5, anti-rab 7, anti-LAMP-1, and anti-Myr 1 (Tu 30) antibodies. Fraction 5 was voluntarily omitted in the pools to clearly delimit pools I and II.

somes and lysosomes (Figure 5D). Endosomes as characterized by the transferrin receptor, the small GTPase rab 5, and a reduced alkaline phosphodiesterase activity were collected in the pool II, whereas lysosomes as characterized by the β-hexosaminidase activity and LAMP-1 were collected in pool I. The small GTPase rab 7, a marker for the late endosomes (Meresse *et al.*, 1995), was predominant in pool I, indicating that this pool was enriched for late endosomes and lysosomes. The bulk of plasma membrane vesicles was recovered

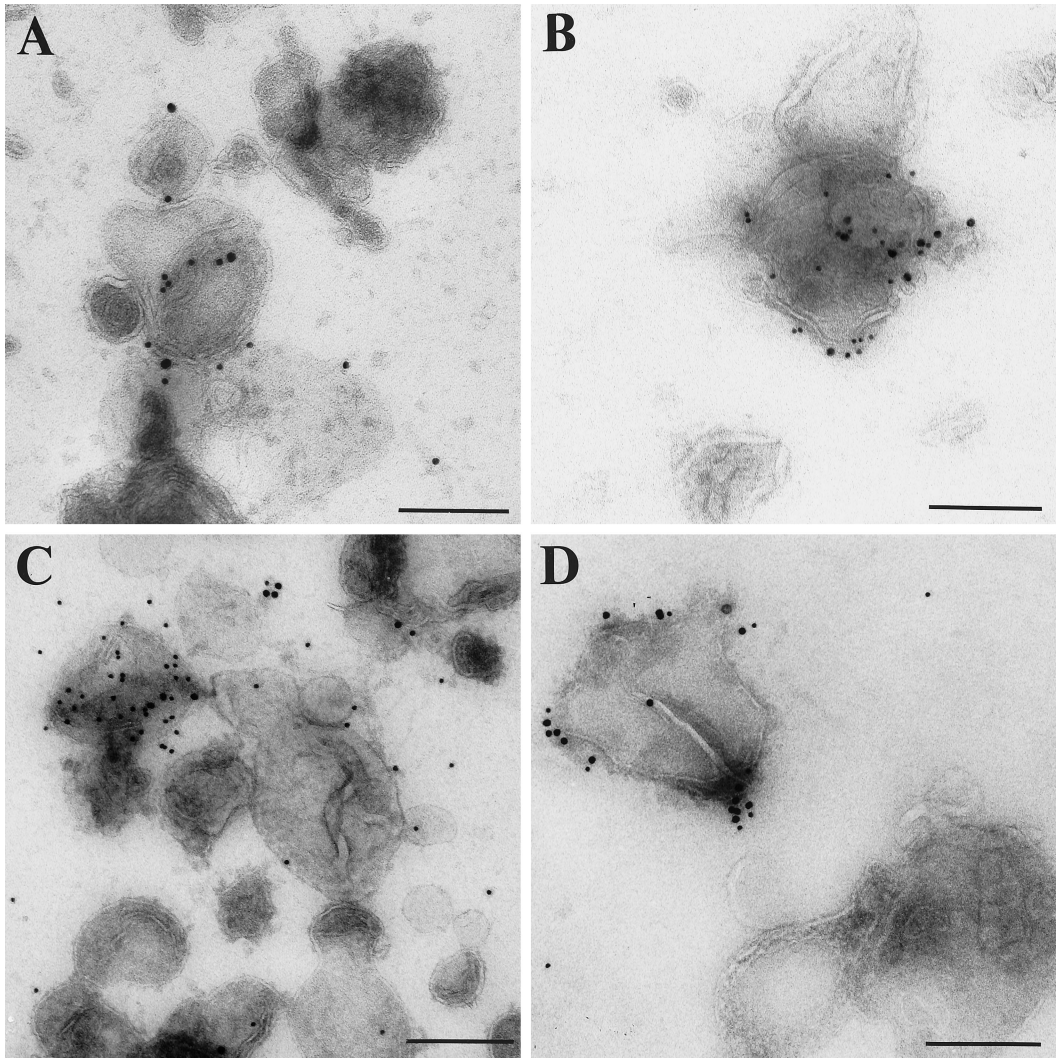

Figure 6. Immunogold labeling of endocytic compartments isolated by sucrose gradient with anti-MMIα antibodies and antibodies directed against specific markers of endocytic compartments (transferrin receptor and lgp 120). Fractions collected after separating the postnuclear supernatant from BWTG3 cells by a sucrose density gradient and enriched in endocytic markers (see Figure 5B, lane E) were loaded onto EM grids. These membrane vesicles were double immunogold labeled (A) with anti-Myr 1 antibodies (Tu 30, PAG 15) and anti-transferrin receptor antibody (PAG 10; B), with anti-Myr 1 antibodies (PAG 15) and anti-cytoplasmic tail lgp 120 antibodies (PAG 10), and (C and D) with anti-BBMI antibody (CX-1; PAG 15) and anti-β-actin antibodies (PAG 10). (D) Cells were treated with cytochalasin D before fractionation. Bars, 200 nm

in pool III. Western blot analysis of these three pools with antibodies directed against the MMIα showed that MMIα was abundant in the pool enriched with the plasma membrane markers but was also present in pools I and II enriched in endosomes and late endosomes- and lysosomes-specific markers (Figure 5D).

MMIα Is Associated with Vesicular Membranes Enriched in Endocytic Markers in the Presence or Absence of Actin

To analyze whether MMIα can be detected on membrane vesicles derived from endocytic compartments, we labeled the membrane fractions isolated by sucrose gradient centrifugation and enriched in endocytic markers with anti-MMIα antibodies and antibodies directed against specific markers of endocytic compartments such as the transferrin receptor and lgp 120. We analyzed them by EM by a whole-mount procedure (Raposo *et al.*, 1996). The majority of vesicles, shown Figure 6, had a mean diameter of 200–300 nm that was compatible with the size of endocytic compartments. In agreement with our observations on whole-mounted cells, some vesicles were double immunogold labeled with anti-MMIα antibodies and an-

ti-transferrin receptor antibody (Figure 6A). Others were double immunogold labeled with anti-MMIα antibodies and anti-cytoplasmic tail lgp 120 antibodies (Figure 6B). A large proportion of these membrane vesicles were also double immunogold labeled with anti-MMIα antibodies and anti-β-actin antibodies (Figure 6C). To analyze whether the detection of MMIα on membrane vesicles depended on actin filaments, cells were treated with cytochalasin D, which impairs the distribution and the structure of actin filaments before the fractionation. In these conditions the number of gold particles corresponding to actin was considerably reduced, whereas the number of gold particles corresponding to MMIα remained similar to the number observed before cytochalasin D treatment (Figure 6, D vs. C).

Altogether, these observations indicate that MMIα is associated with membrane vesicles derived from endocytic compartments, and that this association does not depend on the integrity of actin filaments.

The Overproduction of MMIα or the Production of Truncated MMIα Proteins Affects the Distribution of the Transferrin Receptor

Because a fraction of MMIα is associated with endosomes, we wondered whether MMIα could play a role in endocytosis. Toward this goal, we studied the distribution of the transferrin receptor in cells that overproduced GFP-Myr 1 (the rat MMIα) and two GFP-truncated Myr 1 epitope-tags (GFP-Myr 1Δn295 and GFP-Myr 1-Tail), which were expected to be nonfunctional. Myr 1Δn295 (aa 296-1141) lacks a domain that encompasses the ATP binding site, and Myr 1-Tail (aa 747-1141) lacks the entire motor domain. We expressed GFP-Myr 1 and the GFP-truncated Myr 1 proteins in the hepatoma cells by transient transfections. Likely because of their overproduction, GFP-Myr 1 and the GFP-truncated Myr 1 proteins were highly abundant in the cytoplasm similarly to the GFP itself (Figure 7, A, C, E, and G). The transferrin receptor was concentrated in the pericentriolar region of cells producing GFP (Figure 7, A and B), as previously observed in Figure 2 in untransfected cells. In contrast, it was no longer confined in the pericentriolar region of cells producing GFP-Myr 1, and the GFP-Myr 1 truncated proteins (Figure 7, B, D, F, and H). Instead it appear scattered throughout the cytoplasm. The perinuclear distribution of the transferrin receptor was affected in 1.2% of cells producing the GFP whereas it was affected in 83, 86, and 70% of cells producing GFP-Myr 1, GFP-Myr 1Δn295, and GFP tag Myr 1-Tail, respectively. This experiment indicates that the overproduction of Myr-1, the rat MMIα, as well as the production of truncated Myr 1 proteins can perturb the distribution of the endocytic compartments labeled with transferrin receptor.

BBMI Truncated Proteins Promote the Dissociation of MMIα from Membrane Vesicles

MMIα shares 78% homology with BBMI, another myosin I of the same subclass. We observed previously that BBMI truncated proteins had a dominant negative effect on endocytosis (Durrbach *et al.*, 1996a). As a working hypothesis we postulated that the truncated BBMI proteins might compete with MMIα. Thus, we investigated whether the truncated BBMI proteins could dissociate MMIα from membrane vesicles isolated by the Percoll gradient. Membranes from the three pools described Figure 5 were incubated 2 h with or without identical amount of GST-BBMIΔ446, GST-Tail, or GST alone at 4°C. The distribution of MMIα in soluble fractions and membrane pellets collected after ultracentrifugation was analyzed by Western blots. Although a significant fraction of the GST-truncated BBMI proteins aggregated spontaneously and therefore sedimented independently of the presence of vesicular membrane, a double amount of the recombinant proteins was detected in the pellets when these proteins were incubated with vesicular membrane from pool I, II, or III (our unpublished results). Figure 8 shows that addition of GST-BBMIΔ446 or GST-Tail to membrane vesicles from pool I, II, or III induced the dissociation of some MMIα, whereas addition of GST had no effect. GST-Tail dissociated a similar amount of MMIα from the different pools (Figure 8). Truncated BBMI proteins that cosedimented specifically with vesicular membranes therefore induced the dissociation of MMIα from these membranes, suggesting that the truncated BBMI proteins might affect endocytosis by competing with MMIα in the hepatoma cell line.

BBMI Truncated Proteins Affect the Delivery of Fluid Phase Tracers to Lysosomes

We investigated further the role of MMIα in endocytosis by analyzing at the ultrastructural level the ability of the cells producing the truncated BBMI proteins to internalize HRP by fluid phase as well as to transfer this tracer to the lysosomal compartment.

We first analyzed qualitatively at the electron microscopic level by conventional DAB cytochemistry the distribution of the internalized HRP in mock cells and in cells producing BBMI, BBMIΔ446, or BBMI-Tail. After a 40-min incubation, HRP was detected in mock cells throughout the endocytic pathway in compartments that can be defined by their size and morphology as endosomes and lysosomes (Geuze *et al.*, 1988) (Figure 9A). We observed no significant change in the distribution of internalized HRP in cells producing the entire BBMI protein (our unpublished results). In contrast, in the majority of the cells producing BBMIΔ446 that have internalized HRP, the electron-dense reaction product was only poorly seen in compartments containing in-

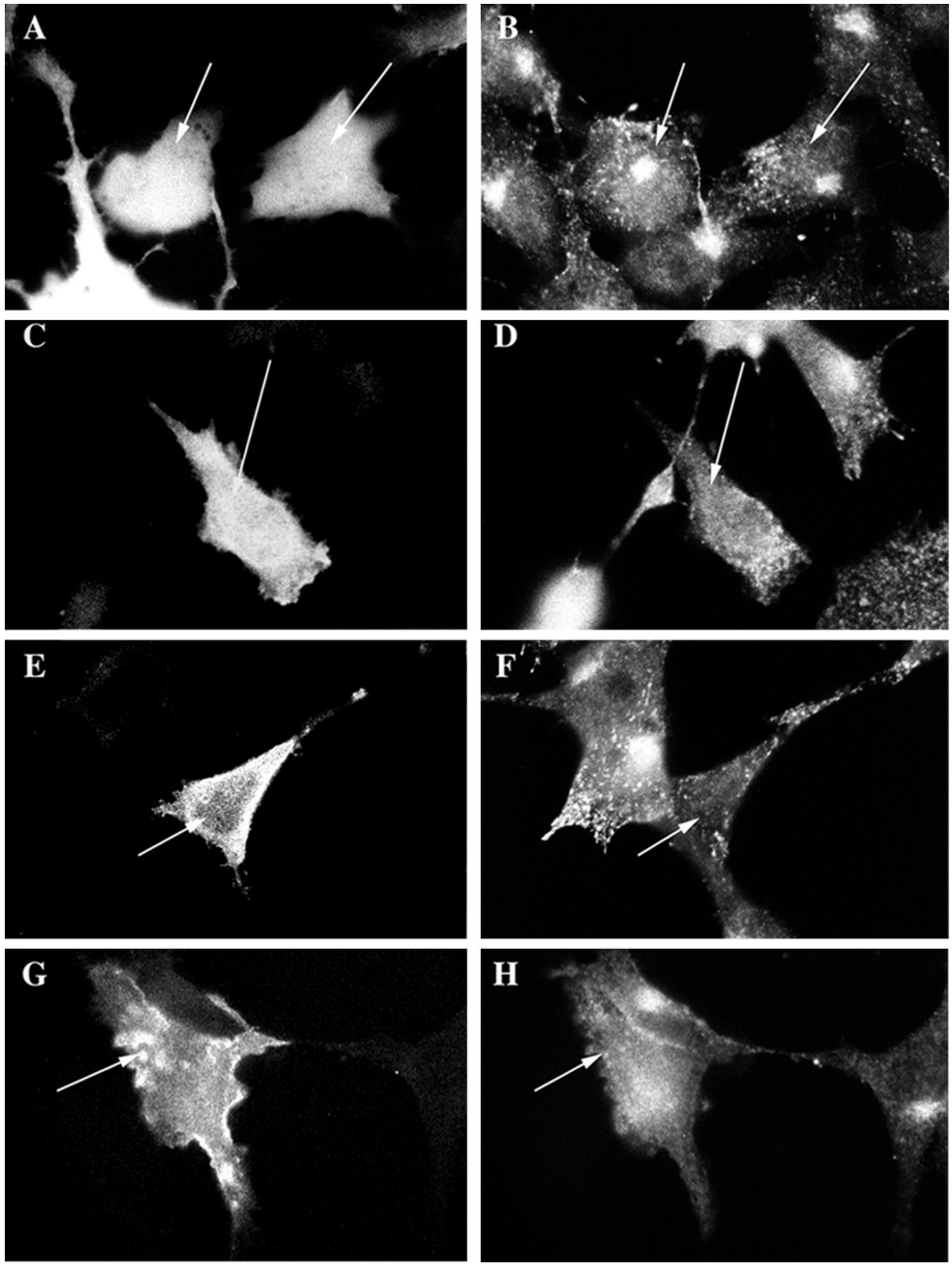

Figure 7. The production of GFP-Myr 1, GFP-Myr 1Δn295, and GFP-Myr 1 tail affects the distribution of transferrin receptor. Twenty-four hours after transfection with cDNA encoding GFP (A and B), GFP-Myr 1 (C and D), GFP-Myr 1Δn295 (E and F), and GFP-Myr 1-Tail (G and H), cells were fixed and permeabilized with saponin. Preparations were analyzed by epifluorescent microscopy, for both the expression of the GFP recombinant proteins (A, C, E, and G) and the distribution of endosomes bearing transferrin receptor (B, D, F, and H). Cells producing GFP proteins are indicated by arrows.

tralumenal membranes, which were morphologically related to lysosomes (Figure 9B). Endocytic compartments including lysosomal compartments from cells producing the tail domain of BBMI contained internalized HRP, although their cellular distribution was affected (our unpublished results). In addition, numerous small vesicles (mean diameter, 100 nm) containing the electron-dense reaction product were visualized underneath the plasma membrane of these cells (Figure 9C). These small

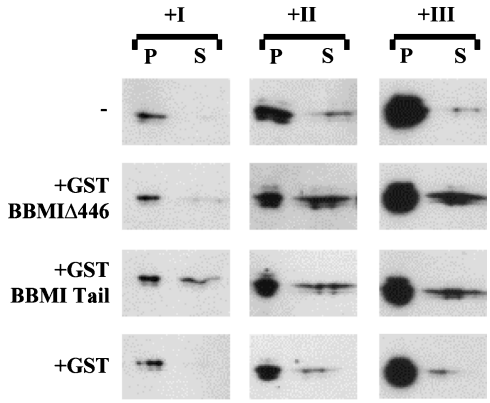

Figure 8. In vitro competition of GST-BBMIΔ446 and GST-BBMI-Tail proteins with the MMIα associated with pools I–III. Membranes contained in the three pools were incubated in PBS at 0.5 mg/ml for 2 h at 4°C alone or with 2 μM GST-BBMIΔ446, GST-BBMI-Tail, or GST. After incubation with the fusion proteins, samples were centrifuged at 300,000 × *g* for 30 min. Proteins recovered from pellets and supernatants were separated by a 7% SDS-PAGE, transferred on nitrocellulose membrane, and probed with anti-MMIα antibodies (Tu 30). Samples loaded correspond to the treatment of 2.5 and 37.5 μg of total membrane proteins for the pellets and the supernatants, respectively.

vesicles were not accessible by fluid phase marker internalized for 5 min (our unpublished results).

We then investigated whether the compartments containing intralumenal membranes but devoid of HRP in cells producing BBMIΔ446, as well as the small vesicles at the periphery of cells producing BBMI-Tail exhibited specific markers of lysosomes. We labeled ultrathin cryosections from the different cell types that had internalized HRP for 40 min using a double immunogold labeling procedure with anti-HRP antibodies and anti-cathepsin D or anti-LAMP-1 antibodies. In cells producing wild-type BBMI, the majority of cathepsin D–enriched compartments (lysosomes) contained high amounts of HRP (Figure 10A). Cathepsin D and HRP exhibited a similar distribution in endocytic compartments of mock cells (our unpublished results). In contrast, in cells producing BBMIΔ446, HRP accumulated mainly in smaller compartments that were only faintly labeled with the anti-cathepsin D antibodies. Conversely, the majority of lysosomes did not contain HRP (Figure 10B). Quantitative analysis of HRP distribution in the lysosomal compartments was performed in these cells and compared with control cells. Because the distribution of so-called lysosomal markers was not only restricted to lysosomes, compartments containing >10 gold particles representing cathepsin D labeling were considered lysosomes (van Weert *et al.*, 1995). The percentage of compartments containing both HRP and cathepsin D was much lower in cells expressing BBMIΔ446 (Figure 11). The morphology of the endocytic compartments in cells expressing BBMIΔ446 per se was not affected, but the transfer of endocytic tracers to the lysosomal compartment was impaired. In cells producing BBMI-Tail, HRP was detected in lysosomes (Figure 10D). Analysis of HRP distribution in the lysosomal compartments showed that the percentage of compartments containing both HRP and cathepsin D in these cells was comparable to control cells (Figure 11). In addition, HRP was detected together with cathepsin D in the small vesicular structures distributed at the cell periphery, underneath the plasma membrane (Figure 10C). Thus, contrary to the expression of BBMIΔ446, the expression BBMI-Tail affects strongly the intracellular distribution of endocytic compartments.

DISCUSSION

MMIα Is Associated with Endosomes and Lysosomes

Our previous data allowed us to postulate that BBMI truncated proteins might compete with an endogenous myosin I involved in late endocytic events. In agreement with this hypothesis, in the present study we show that a closely related myosin I of this subclass MMIα is detected on endosomes and lysosomes. Monoclonal antibodies directed against the motor domain of BBMI and polyclonal antibodies directed against the rat MMIα (Myr 1) both immunoprecipitate a 130-kDa protein in the BWTG3 cells. Mass spectrometry analysis of the peptides generated by trypsin proteolysis of this protein revealed that it was MMIα. Using polyclonal antibodies specifically recognizing MMIα in the BWTG3 cells, we show by immunocytochemistry at the light and electron microscopic level that MMIα is distributed near the plasma membrane and with endosomes and lysosomes of these cells. The analysis of its distribution after cell fractionation indicates also that a fraction of MMIα is associated with vesicular membrane derived from endocytic compartments. Indeed it is unlikely that the amount of MMIα detected in the pool enriched for endocytic markers (pool II) corresponds only to a contamination of this pool by plasma membrane. The alkaline phosphodiesterase activity recovered in pool II represented 28% of the activity detected in pool III enriched for plasma membrane vesicles, whereas the amount of MMIα in this pool represented 50% of the amount detected in pool III. Furthermore, immunoelectron microscopic analysis of these fractions has shown that MMIα was detected together with endocytic markers on the membrane vesicles in an actin-independent manner.

MMIα Is a Likely Candidate to Participate in the Delivery of Endocytic Tracers from Endosomes to Lysosomes

Myr 1, the rat MMIα, Myr 1Δn295 (deleted of the amino-terminal domain encoding the ATP binding

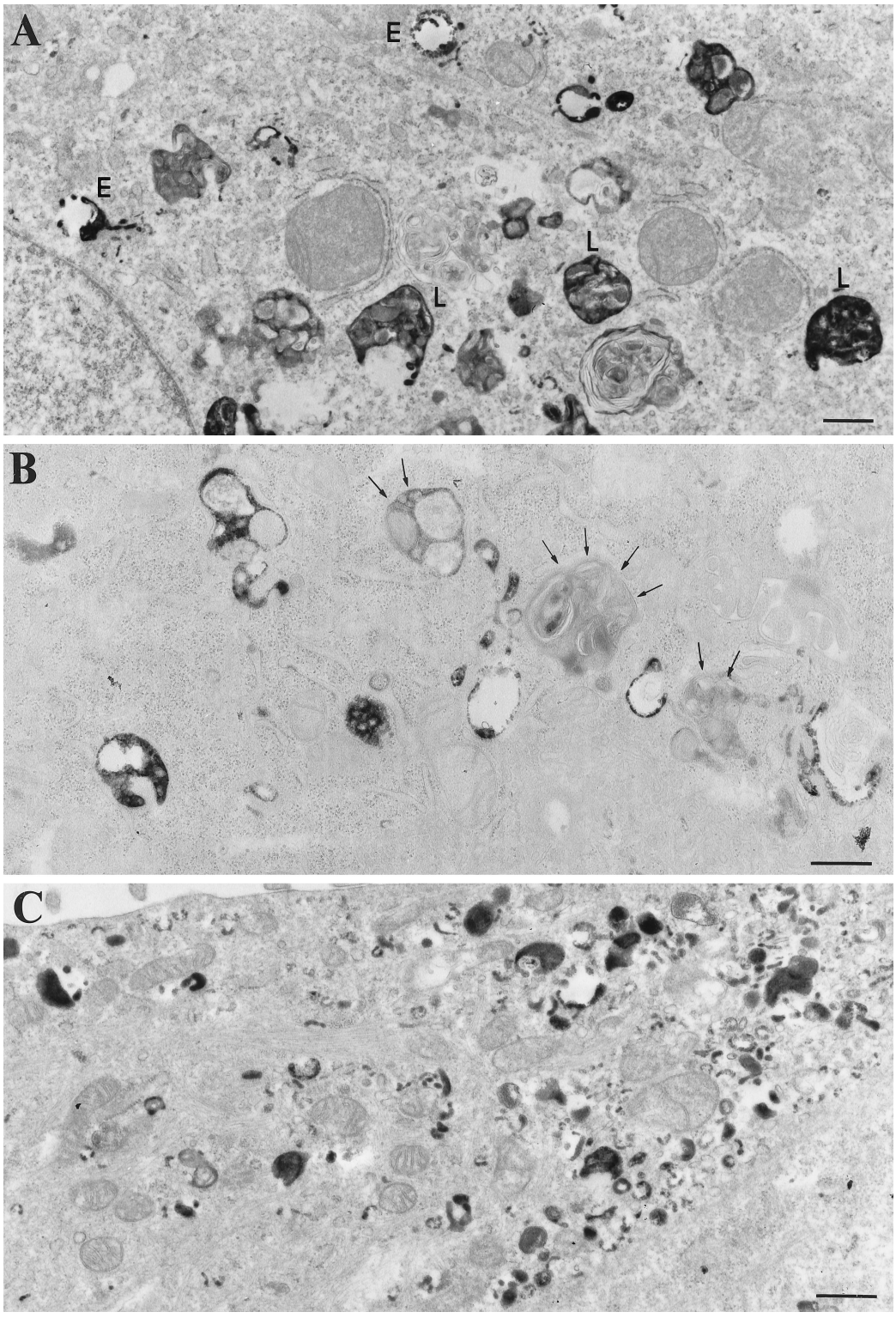

Figure 9. Internalization of HRP by BWTG3 mock cells and cells producing BBMIΔ446 and BBMI-Tail. Cells were allowed to internalize HRP for 40 min at 37°C, fixed, and processed for DAB cytochemistry and conventional EM. In mock-treated cells (A) the electron-dense DAB reaction product was detected in intracellular compartments, which were morphologically related to endosomes (E) and lysosomes (L). In cells producing BBMIΔ446 (B), lysosomal-like compartments were devoid of electron-dense reaction product (arrows). In cells overexpressing BBMI-Tail (C), the reaction product accumulated in small vesicles distributed beneath the plasma membrane. Bars, 100 nm.

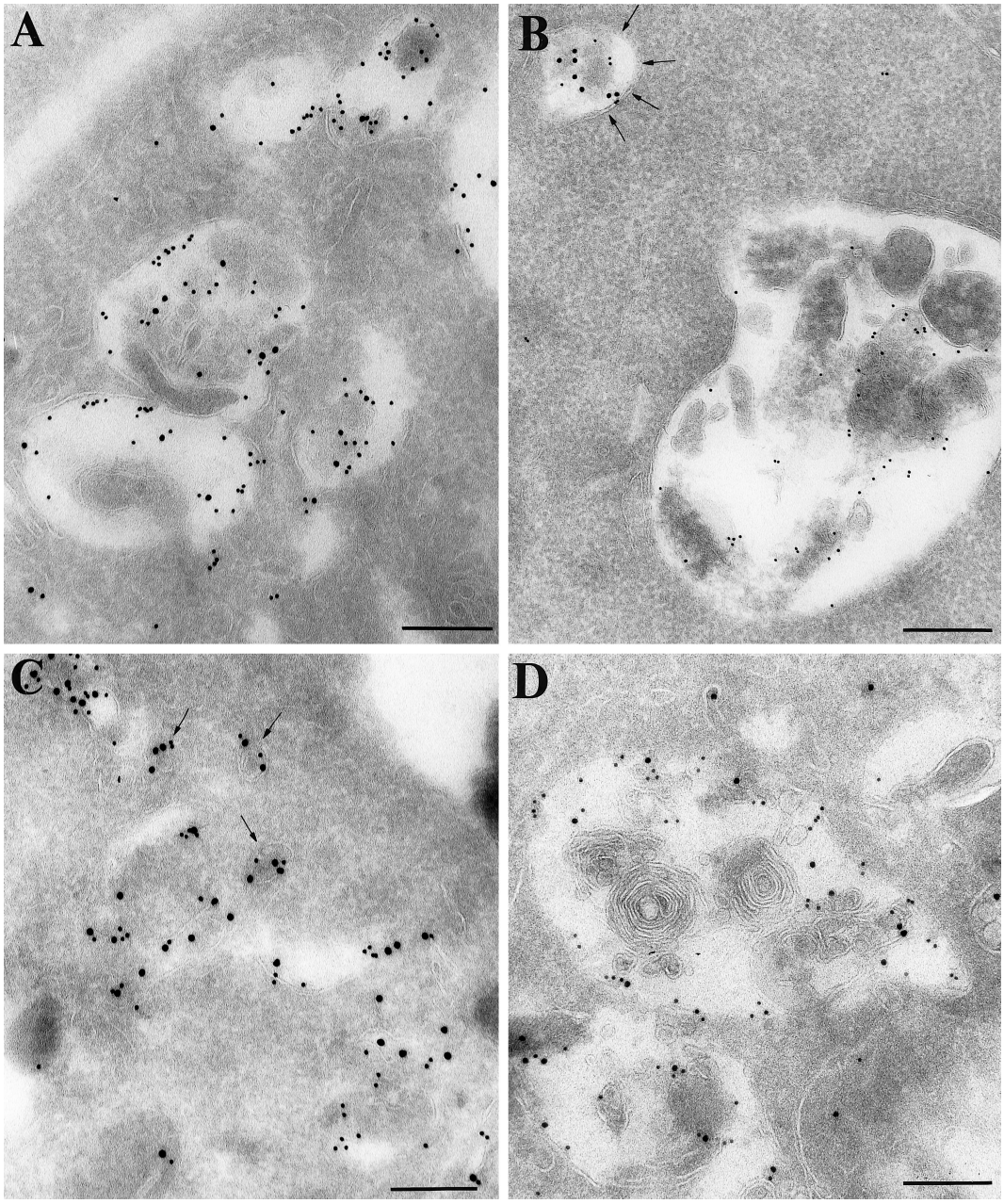

Figure 10. Immunogold localization of HRP (PAG 15) and cathepsin D (PAG 10) on ultrathin cryosections of BWTG3 cells producing BBMI (A), BBMIΔ446 (B), and BBMI-Tail (C and D). Before fixation cells were allowed to internalize HRP for 40 min at 37°C. In cells producing wild-type BBMI (A), the majority of cathepsin D-positive compartments contained large amounts of HRP. On the opposite, in cells producing BBMIΔ446 (B), HRP mostly accumulated in smaller compartments that were faintly labeled with the anti-cathepsin D antibodies (arrows), and the majority of lysosomes did not contain HRP. In cells overexpressing BBMI-Tail, HRP was detected in lysosomes (D) and in small cathepsin D-positive vesicular structures that were distributed at the cell periphery beneath the plasma membrane (C, arrows). Bars, 200 nm.

site), and Myr 1-Tail (deleted of the motor domain) affect the pericentriolar distribution of the transferrin receptor. Although we cannot rule out that the fraction of MMIα located near the plasma membrane might participate in other cellular processes such as cell motility, the fraction of MMIα that is associated with endosomes might therefore be involved in the endocytic process. Myr 1 shares 78% homology with BBMI. Similarly to the truncated Myr 1 proteins, nonfunctional BBMI proteins affect the distribution of the endocytic compartments when they are produced in the hepatoma cell line (Durrbach *et al.*, 1996a). They

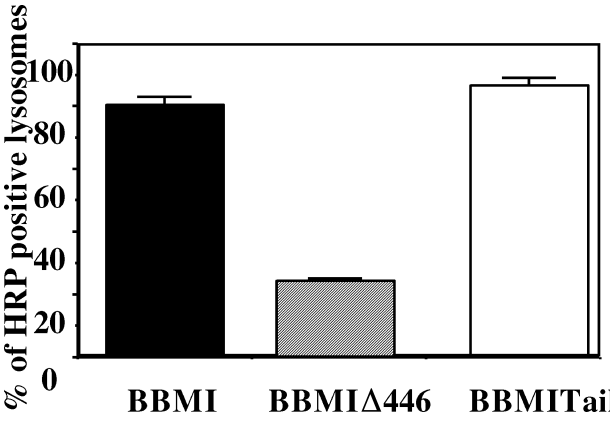

Figure 11. Semi-quantitative analysis of immunogold labeling for HRP and cathepsin D on ultrathin cryosections of cells producing BBMI, BBMIΔ446, and BBMI-Tail. Cathepsin D-positive compartments that contained more than 10 gold particles (lysosomes) were screened for the presence of HRP. Errors bars represent the SD calculated for two independent experiments.

also affect the distribution of the endogenous MMIα (Coudrier, unpublished data). Furthermore, they promote the dissociation of MMIα from membrane derived from endocytic compartments. Altogether these observations support our hypothesis that the truncated BBMI proteins have a dominant negative effect on endocytosis by competing with an endogenous myosin I, namely MMIα. The analysis at the ultrastructural level of the cells producing the truncated BBMI proteins revealed that BBMIΔ446 affects the delivery of the fluid phase markers to lysosomes. This observation is in agreement with our previous observations indicating that BBMIΔ446 decreased the rate of degradation of the α2-macroglobulin. BBMI-Tail affects the distribution and/or the morphology of endocytic compartments. We observed a large number of small vesicles at the cell periphery that were positive for cathepsin D. This observation supports our previous data showing that BBMI-Tail increased the rate of degradation of the α2-macroglobulin. They suggest that MMIα associated with endocytic compartments contributes to the endocytic process by controlling the delivery of ligands from endosomes to lysosomes.

MMIα is the first mammalian myosin I for which experimental evidence suggests that it controls a late step of the endocytic process. The double deletion of the myo 3 and myo 5 genes encoding the two myosin Is in yeast *S. cerevisiae* leads to a defect in the uptake of ligand during receptor-mediated endocytosis (Geli and Riezman, 1996; Goodson *et al.*, 1996). However, in contrast to BBMI and MMIα, these two myosins exhibit an ATP-independent actin binding site in their tail, and mutants deleted for the two genes exhibit a severe defect in actin cytoskeletal organization. Although a myosin I homologous to Myo 3 and Myo 5 has not yet been described in mammals, one can postulate that two different acto-myosin–based mechanisms involving different subclasses of myosin I might control two different steps of endocytosis. Myosin I from the Myo 3–Myo 5 subfamily might participate in a dynamic reorganization of the cortical actin cytoskeleton required for the internalization step of receptor-mediated endocytosis, whereas MMIα might control a later step of the receptor-mediated and fluid phase endocytic pathways.

How Might the Acto-Myosin System Contribute to the Delivery of Ligands from Endosomes to Lysosomes?

Three different models have been proposed for the transfer of internalized molecules along the endocytic pathway and the biogenesis of endosomes and lysosomes. Early endosomes may gradually mature into late endosomes and lysosomes (Roederer *et al.*, 1990; Murphy, 1991). Alternatively, the maturing endosomes may fuse with preexisting lysosomes (Stoorvogel *et al.*, 1991; Futter *et al.*, 1996; Mullock *et al.*, 1998). A third model suggests that endocytosed molecules may be transported from early endosomes to preexisting late endosomes and lysosomes by vesicular transport (Griffiths and Gruenberg, 1991). According to the first model, important morphological changes are required to form lysosomes with their characteristic multilamellar structures from late endosomes. It is unlikely that MMIα is involved in such morphological changes, because mature lysosomes are also present in cells producing BBMI-truncated proteins. Taking in consideration the second and third models, MMIα and actin may be essential for the close apposition of endosomes and/or small transport vesicles with lysosomes. MMIα might tether these membrane domains to actin filaments similarly to BBMI in the microvilli (Matsudaira and Burgess, 1979; Drenckhahn and Dermietzel, 1988). Indeed, it is tempting to speculate that the thin filaments described in between closely apposed late endosomes and lysosomes contain actin and MMIα (Futter *et al.*, 1996). By binding endosomes or endocytic vesicles transiently to actin filaments, MMIα might thereby participate to the fusion process.

According to this hypothesis, BBMIΔ446, which lacks the ATP binding site, will compete with MMIα to bind endosomes to actin filaments. However, because this complex will be unable to release endosomes in an ATP-dependent manner from the actin filaments, it will thereby prevent fusion to process normally. In contrast, BBMI-Tail, which lacks the ATP and the actin binding site, will compete with MMIα to inhibit the interaction of endosomes with actin filaments. Consequently, it may alter the architectural organization of the endocytic compartments and

thereby increase the number of random fusion events between endosomes and lysosomes occurring by default of a normally tightly regulated mechanism.

Important questions that remain to be solved are whether the binding of endosomes on actin filaments via the MMIα in vivo lead to the generation of a force able to induce vesicular movements between late endosomes and lysosomes or is involved in morphological changes of endosomal membranes such as formation of buds and vesicles. Further structural studies as well as detailed analysis of MMIα kinetics and mechanics itself will be required to answer to these questions.

ACKNOWLEDGMENTS

We thank Dr. W. Stoorvogel (University of Utrecht, Utrecht, The Netherlands) for helpful advice to apply his whole-mount EM method to the BWTG3 cells, M. Grasset (University Paris VI, Paris, France) for help with critical point drying, and J. P. Le Caert (Ecole Supérieure de Physique-Chimie de la Ville de Paris, Paris, France) for contribution and helpful advice with the mass spectrometry analysis. We are grateful to Dr. M. Bähler (Ludwig Maximilian University, Munich, Germany) for the generous gift of antibodies as well as for critically reading the manuscript and Dr. R. Golsteyn (Institut Curie, Unité Mixte de Recherche 144, Paris, France) for critically reading the manuscript. We also thank Drs. M. Mooseker (Yale University, New Haven, CT), N. Andrews (Yale University), C. Chaponnier (Geneva University, Geneva, Switzerland), M. Zerial (European Molecular Biology Laboratory, Heidelberg, Germany), M. Bornens (Institut Curie, Unité Mixte de Recherche 144), and P. Chavrier (Institut National de la Santé et de la Recherche Médicale–Centre National de la Recherche Scientifique [CNRS], Marseille, France) for the generous gifts of antibodies. D. Meur and D. Morineau (Institut Curie, UMR 144) are acknowledged for their photographic assistance. This work was supported by Human Capital and Mobility (European Community grant CHRX CT 94-0430), and the CNRS (Biologie Cellulaire du normal au pathologique grant 385024).

REFERENCES

Bailly, E., Favel, J., Mahouy, G., and Jaureguyberry, G. (1991). *Plasmodium falsiparum*: isolation and characterization of a 55 kDa protease with cathepsin like activity from *Plasmodium falsiparum*. Exp. Parasitol. *72*, 278–284.

Baker, J.P., and Titus, M.A. (1998). Myosins: matching functions with motors. Curr. Opin. Cell Biol. *10*, 80–86.

Bakker, A.C., Webster, P., Jacob, W.A., and Andrews, N.W. (1997). Homotypic fusion between aggregated lysosomes triggered by elevated (Ca2+) in fibroblasts. J. Cell Sci. *110*, 2227–2238.

Bearer, E., DeGiorgis, J., Jaffe, H., Medeiros, N., and Reese, T. (1996). An axoplasmic myosin with a calmodulin-like light chain. Proc. Natl. Acad. Sci. USA *12*, 6064–6068.

Bement, W.M., Hasson, T., Wirth, J.A., Cheney, R.E., and Mooseker, M.S. (1994). Identification and overlapping expression of multiple unconventional myosin genes in vertebrate cells types. Proc. Natl. Acad. Sci. USA *91*, 6549–6553.

Carboni, J.M., Conzelman, K.A., Adams, R.A., Kaiser, D.A., Pollard, T.D., and Mooseker, M.S. (1988). Structural and immunological characterization of the myosin-like 110-kDa subunit of the intestinal microvillar 110k-calmodulin complex: evidence for discrete myosin head and calmodulin binding domains. J. Cell Biol. *107*, 1749–1757.

Chavrier, P., Parton, R., Hauri, H., Simons, K., and Zerial, M. (1990). Localization of low molecular weight GTP binding proteins to exocytic and endocytic compartments. Cell *62*, 317–329.

Coluccio, M.L., and Conaty, C. (1993). Myosin-I in mammalian liver. Cell Motil. Cytoskeleton *24*, 189–199.

Cope, M.J.T., Whisstock, J., Rayment, I., and Kendrick-Jones, J. (1996). Conservation within the myosin motor domain: implications for structure and function. Structure *4*, 969–987.

Drenckhahn, D., and Dermietzel, R. (1988). Organization of the actin filaments cytoskeleton in the intestinal brush-border: a quantitative and qualitative immunoelectron microscope study. J. Cell Biol. *107*, 1037–1048.

Durrbach, A., Collins, K., Matsudaira, P., Louvard, D., and Coudrier, E. (1996a). Brush border myosin-1 truncated in the motor domain impairs the distribution and the function of endocytic compartments in a hepatoma cell line. Proc. Natl. Acad. Sci. USA *93*, 7073–7058.

Durrbach, A., Louvard, D., and Coudrier, E. (1996b). Actin filaments facilitate two steps of endocytosis. J. Cell Sci. *109*, 457–465.

Evans, L.L., and Bridgman, P.C. (1995). Particles move along actin filament bundles in nerve growth cones. Proc. Natl. Acad. Sci. USA *92*, 10954–10958.

Evans, L.L., Lee, J.A., Bridgman, P.C., and Mooseker, M.S. (1998). Vesicles-associated brain myosinV can be activated to catalyze actin based transport. J. Cell Sci. *111*, 2055–2066.

Futerman, A.H., Stieger, B., Hubbard, A.L., and Pagano, R.E. (1990). Sphingomyelin synthesis in rat liver occurs predominantly at the *cis* and medial cisternae of the Golgi apparatus. J. Cell Biol. *106*, 77–86.

Futter, C., Pearse, A., Hewlett, L.J., and Hopkins, C.R. (1996). Multivesicular endosomes containing internalized EGF-EGF receptor complexes mature and then fuse directly with lysosomes. J. Cell Biol. *132*, 1011–1023.

Geli, M.I., and Riezman, H. (1996). Role of type I myosins in receptor-mediated endocytosis in yeast. Science *272*, 533–535.

Geuze, H.J., Stoorvogel, W., Strous, G.J., Slot, J.W., Bleekemolen, J.E., and Mellman, I. (1988). Sorting of mannose-6-phosphate receptors and lysosomal membrane proteins in endocytic vesicles. J. Cell Biol. *107*, 2491–2501.

Goodson, H., Anderson, B., Warrick, H., Pon, L., and Spudich, J. (1996). Synthetic lethality screen identifies a novel yeast myosin I gene (myo5): myosin I proteins are required for polarization of the actin cytoskeleton. J. Cell Biol. *133*, 1277–1291.

Goodson, H.V., and Spudich, J.A. (1995). Identification and molecular characterization of a yeast myosin I. Cell Motil. Cytoskeleton *30*, 73–94.

Gorvel, J.P., Chavrier, P., Zerial, M., and Gruenberg, J. (1991). Rab 5 controls early endosome fusion in vitro. Cell *64*, 915–925.

Green, S.A., Zimmer, K.-P., Griffiths, G., and Mellman, I. (1987). Kinetics of intracellular transport and sorting of lysosomal membrane and plasma membrane proteins. J. Cell Biol. *105*, 1227–1240.

Griffiths, G., and Gruenberg, J. (1991). The arguments for preexisting early and late endosomes. Trends Cell Biol. *1*, 5–10.

Jasmin, B.J., Cartaud, J., Bornens, M., and Changeux, J.P. (1989). Golgi apparatus in chick skeletal muscle: changes in its distribution during end plate development and after denervation. Proc. Natl. Acad. Sci USA *86*, 7218–7222.

Jung, G., Wu, X., and Hammer, J.A., III (1996). *Dictyostelium* mutants lacking multiple classic myosin I isoforms reveal combinations of shared and distinct functions. J. Cell Biol. *133*, 305–323.

Langford, G., Kutnetsov, S., Johnson, D., Cohen, D., and Weiss, D. (1994). Movement of axoplasmic organelles on actin filaments as-

sembled on acrosomal process: evidence for barbed end directed organelle motor. J. Cell Sci. *107*, 2291–2298.

Lewis, A.K., and Bridgman, P.C. (1996). Mammalian myosin Ia is concentrated near the plasma membrane in nerve growth cones. Cell Motil. Cytoskeleton *33*, 130–150.

Matsudaira, P.T., and Burgess, D.R. (1979). Identification and organization of the components in the isolated microvillus cytoskeleton. J. Cell Biol. *83*, 667–673.

McGoldrick, C.A., Gruver, C., and May, G.S. (1995). *myoA* of *Aspergillus nidulans* encodes an essential myosin I required for secretion and polarized growth. J. Cell Biol. *128*, 577–587.

Meresse, S., Gorvel, J., and Chavrier, P. (1995). The rab7 GTPase resides on a vesicular compartment connected to lysosomes. J. Cell Sci. *108*, 3349–3358.

Mermall, V., and Miller, K. (1995). The 95F unconventional myosin is required for proper organization of the drosophila syncytial blastoderm. J. Cell Biol. *129*, 1575–1588.

Mermall, V., Post, P., and Mooseker, M. (1998). Unconventional myosins in cell movement, membrane traffic, and signal transduction. Science *279*, 527–533.

Morris, R., and Hollenbeck, P. (1995). Axonal transport of mitochondria along microtubules and F-actin in living vertebrate. J. Cell Biol. *131*, 1315–1326.

Mullock, B.M., Bright, N.A., Fearon, C.W., Gray, S.R., and Luzio, J.P. (1998). Fusion of lysosomes with late endosomes produces a hybrid organelle of intermediate density and is NSF dependent. J. Cell Biol. *140*, 591–601.

Murphy, R.F. (1991). Maturation models for endosome and lysosome biogenesis. Trends Cell Biol *1*, 77–82.

Musch, A., Cohen, D., and Rodriguez-Boulan, E. (1997). Myosin II is involved in the production of constitutive transport vesicles from the TGN. J. Cell Biol. *138*, 291–306.

Novak, K.D., Peterson, M.D., Reedy, M.C., and Titus, M.A. (1995). *Dictyostelium* myosin I double mutants exhibit conditional defects in pinocytosis. J. Cell Biol. *131*, 1205–1221.

Novak, K.D., and Titus, M.A. (1997). Myosin I overexpression impairs cell migration. J. Cell Biol. *136*, 633–647.

Ostap, M.E., and Pollard, T.D. (1996). Overlapping functions of myosin-I isoforms. J. Cell Biol. *133*, 221–224.

Raposo, G., Kleijmeer, M.J., Posthuma, G., Slot, J.W., and Geuze, H.J. (1997). Immunogold labeling of ultrathin cryosections: application in immunology. In: Weir's Handbook of Experimental Immunology, 5th ed., vol. 4, ed. L.A. Herzenberg, D. Weir, and C. Blackwell, Cambridge, MA: Blackwell Science, 1–11.

Raposo, G., Nijman, H.W., Stoorvogel, W., Leijendekker, R., Harding, C.V., Melief, C.J.M., and Geuze, H.J. (1996). B lymphocytes secrete antigen-presenting vesicles. J. Exp. Med. *183*, 1161–1172.

Roederer, M., Barry, J.R., Wilson, R.B., and Murphy, R.F. (1990). Endosomes can undergo an ATP-dependent density increase in the absence of dense lysosomes. Eur. J. Cell Biol. *51*, 229–234.

Rogers, S., and Gelfand, V.S. (1998). Myosin cooperates with microtubule motors during organelle transport in melanophore. Curr. Biol. *8*, 161–164.

Ruppert, C., Godel, J., Muller, R.T., Kroschewski, R., Reinhard, J., and Bahler, M. (1995). Localization of the rat myosin I molecules myr 1 and myr 2 and in vivo targeting of their tail domains. J. Cell Sci. *108*, 3775–3786.

Ruppert, C., Kroschewski, R., and Bahler, M. (1993). Identification, characterization and cloning of myr 1, a mammalian myosin-1. J. Cell Biol. *120*, 1393–1403.

Sheer, E.H., Joyce, M.P., and Greene, L.A. (1993). Mammalian myosin Ia, Ib, Ig: new widely expressed genes of the myosin I family. J. Cell Biol. *120*, 1405–1416.

Shevchenko, A., Wilm, M., Vorm, O., and Mann, M. (1996). Mass spectrometric sequencing of proteins from silver-stained polyacrylamide gels. Anal. Chem. *68*, 850–858.

Simon, J., Shen, T., Ivanov, I., Gravotta, D., Morimoto, T., Adesnik, M., and Sabatini, D. (1998). Coatomer, but not P200/myosin II, is required for the in vitro formation of trans-Golgi network-derived vesicles containing the envelope glycoprotein of vesicular stomatitis virus. Proc. Natl. Acad. Sci. USA *95*, 1073–1078.

Slot, J.W., Geuze, H.J., Gigengack, S., Lienhard, G.E., and James, D. (1991). Immuno-localization of the insulin regulatable glucose transporter in brown adipose tissue of the rat. J. Cell Biol. *113*, 123–135.

Stoorvogel, W., Oorschot, V., and Geuze, H.J. (1996). A novel class of clathrin-coated vesicles budding from endosomes. J. Cell Biol. *132*, 21–33.

Stoorvogel, W., Strous, G.J., Geuze, H.J., Oorschot, V., and Schwartz, A.L. (1991). Late endosomes derive from early endosomes by maturation. Cell *65*, 417–427.

Szpirer, C., and Szpirer, J. (1975). A mouse hepatoma cell line which secretes several serum proteins including albumin and α-foetoprotein. Differentiation *4*, 85–91.

van Weert, A.W., Dunn, K.W., Geuze, H.J., Maxfield, F.R., and Stoorvogel, W. (1995). Transport from late endosomes to lysosomes, but not sorting of integral membrane proteins in endosomes, depends on the vacuolar proton pump. J. Cell Biol. *130*, 821–834.

White, S., Miller, K., Hopkins, C., and Trowbridge, I.S. (1992). Monoclonal antibodies against defined epitopes of the human transferrin receptor cytoplasmic tail. Biochem. Biophys. Acta *1136*, 28–34.